Scattering and absorption in 2D optics

Mariani, F.

Scattering of guided light by a single hole in a dielectric slab

We study the scattering of waveguided light by a single hole in a dielectric slab with FDTD simulations and investigate two scattering processes: two dimensional (2D) scattering into slab modes and three-dimensional (3D) scattering into the surroundings. We find that 2D scattering tipically dominates over the 3D losses. We find important quantitative differences between the single hole scattering and the case of scattering from an infinite Mie cylinder. Additionally, we find that a hole cannot be simply modelled as a dipolar object even in the limit of small scatterers (Rayleigh approximation). This is visible from the angular dependence of the 2D scattered intensity. We discuss the relevance of our findings in the modelling of two dimensional random scattering media.

This chapter is published as:
F.Mariani, M.P. van Exter, Optics Express **23**, 17539 (2015).

2.1 2D optics in dielectric slabs

Dielectric membranes are popular substrates for nano-photonic applications [1, 2, 3]. They confine light in two dimensions acting as a waveguide if embedded in a lower refractive index material. Additional spatial control can be achieved by nano-structuring the planar geometry with arrangements of scatterers such as nano-holes. In this way two dimensional photonic crystals [4] are obtained in dielectric membranes and interesting phenomena like photonic bandgaps can appear with proper tuning of the geometry [5, 6], allowing the design of integrated optical circuits with membrane based components like waveguides and cavities [7, 8].

Two dimensional optics is in general subject to losses, caused by material absorption, for instance by defects, or by imperfect nano-structuring of the membrane. Limits in the fabrication process can introduce positional disorder of the scatterers and interface roughness; both of these scatter light outside the waveguide into radiative modes which act as losses for the 2D system. The losses have been calculated by modelling the scattering due to position and shape disorder [9] and roughness via the polarizability of small scatterers [10, 11].

Beside fabrication imperfections, also a geometrically perfect hole gives rise to radiative losses. A hole in a dielectric slab is a discontinuity in the waveguide and can thus scatter light both in the slab (2D scattering) and in the third dimension (3D scattering), determining effective losses. The scattering properties of round holes in dielectric environment have been calculated for simplified geometries, like slits in a slab [12] , infinitely long cylinders [13, 14, 15] and periodic lattices of holes [16, 17], where the first two geometries effectively reduce the dimension of the problem from 3D to 2D.

Although an analytic approach to the scattering from a hole in a layered structure, based on cylindrical mode expansion, is presented in [16], a more descriptive study on the scattering from a single hole in a free standing membrane is still missing. As we will show in the following, a hole in a slab is an interesting system and even for sub-wavelength holes (Rayleigh limit), the radiation profile doesn't resemble that of a radiating dipole in a slab. This finding is in contrast with the result obtained for infinitely long Mie cylinders and the scattering expected for sub-wavelength objects in a uniform 3D medium. Both these scattering processes are dipolar and can be analyzed by treating the scatterer as a polarizable object, even in the case of a hollow

inclusion in an otherwise uniform medium. A similar comparison with a complementary scattering system is less straightforward for the hole in a dielectric slab.

Understanding single hole scattering properties is essential for the description of two dimensional random scattering media. In these systems the field structure is difficult to calculate and it becomes necessary to introduce average transport properties [14, 18] and to use statistical approaches or simulations [19, 20]. The knowledge of the 2D and 3D scattering properties of individual holes could help to simplify the random scattering problem from a full 3D to a 2D problem with effective losses, for a less time consuming calculation of scattering properties.

In this work we use Finite Difference Time Domain (FDTD) simulations to study small holes in a dielectric slab under the excitation of guided light. After introducing our system in Sec. 2.2, we discuss our results for different hole diameters and mode confinements (Sec. 2.3.1) and describe two scattering processes: the 2D scattering in the slab and the 3D scattering in form of freely propagating radiative modes (Sec 2.3.2). We calculate the dependence of the scattering cross section on the hole diameter and the relative role of radiative losses with respect to in-plane scattering. Finally, we examine the angular distribution of the scattered intensity (Sec. 2.3.3) and compare it to the distribution expected for the case of a cylinder in the Rayleigh regime. We apply our results to the calculation of mean free path in random scattering media (Sec. 2.4).

2.2 Simulation method and scattering parameters

We consider the symmetric case of a thin film of dielectric material of real refractive index n_2, surrounded on both sides by a medium with $n_1 < n_2$. The film is oriented with its normal along the z-axis and extends for $-h/2 < z < h/2$, where h is the thickness of the slab. The slab contains a cylindrical hole of diameter d and index n_1 centred at the origin of the Cartesian reference. The problem is described by three relevant physical quantities: the relative refractive index of the material $n = n_2/n_1$, the slab thickness h and the hole diameter d. Without loss of generality, in the rest of the work we set $n_1 = 1$ and express h and d in units of λ_0, the wavelength of the light in vacuum.

Under the condition $n_1 < n_2$, a slab supports guided field modes satisfying the (roundtrip) condition $2h\sqrt{n_2^2 k_0^2 - \beta^2} + 2\phi_\mu(\beta) = 2\pi m$, where k_0 is the

wavevector in vacuum, β is the in-plane component of the wavevector, μ is the field polarization, and $\phi_\mu(\beta)$ is the polarization dependent phase acquired upon total internal reflection at the slab-cladding interface [21]. For the polarization μ we use the convention of indicating with TM (TE) the field with magnetic (electric) field parallel to the plane of the waveguide. The integer modal index m assumes values which depend on the slab geometry: the number of allowed modes increases with slab thickness and in the case of symmetric slabs one TM and one TE mode are always present. We choose the thickness of our slab such that it only supports these two fundamental $m = 0$ modes. This condition simplifies our description and is also the typical situation in membrane-based optics.

We will compare the scattering from a single hole in the waveguide with the Mie theory for scattering of a plane wave from an infinitely long cylinder. In the latter case, the symmetry of problem allows expanding the electromagnetic field in cylindrical harmonics to obtain exact scattering functions [22], but this approach doesn't apply to our geometry. A hole in a slab is also different from a finite size cylinder excited by a plane wave [23, 24]. The main distinctive aspects are: (i) the vertical translational symmetry of the Mie case is missing in a thin film, (ii) the field incident on the hole in the slab is not a plane wave but has a varying amplitude across the hole and an evanescent field portion extending outside the slab, (iii) the hole has end faces that are not present in the Mie cylinder and can contribute to the scattering. Given the peculiar geometry of our problem, we choose a numerical approach.

We describe the scattering processes using the scattering efficiencies Q. These are dimensionless numbers defined as the ratio of scattering cross section and geometrical cross section. Taking into account a portion of length L of an infinitely extended cylinder of diameter d, the scattering efficiency Q_{sca} in the Mie case is:

$$Q_{sca} = \frac{\sigma_{sca}}{d\,L} = \frac{W_s}{I_i\,d\,L} \tag{2.1}$$

where I_i $[W/m^2]$ is the intensity of the incident wave, W_s $[W]$ is the power scattered by the cylinder portion and σ_{sca} $[m^2]$ its scattering cross section. We will modify Eq. (2.1) to account for the two-dimensional confinement of our problem. As for the scattering of surface plasmons from holes in a metal slab [25], we choose the cross section to have dimension of a length and we have:

$$Q_{2D} = \frac{\sigma_{2D}}{d} = \frac{W_{2D}}{\tilde{I}_i\,d} \tag{2.2}$$

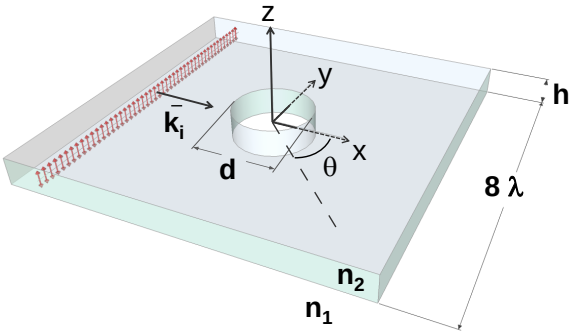

Figure 2.1: The simulation cell is $(8\lambda)^3$ in volume and surrounded by a λ-thick perfectly matching layer.

where $\tilde{I}_i$ $[W/m]$ is the intensity of the incident guided mode per unit length of the wavefront. The same definition holds for radiative losses into free space with the substitution $2D \rightarrow 3D$. Scattering efficiencies are in general polarization dependent but we do not indicate this explicitly in the notation.

2.3 2D scattering in the slab and 3D losses

In this section we present results obtained from simulations performed with the finite-difference time-domain (FDTD) method [26], using the freely available software package MEEP [27]. We simulate the scattering from a hole in a slab with refractive index $n_2 = 1.5$ and hole diameter chosen in the range $0.075 < d < 1.2$. We use slab thicknesses of $h = 0.25, 0.32, 0.40$, all below the cut-off for the appearance of the higher-order TM and TE modes. The simulation cell used for this work is shown in Fig. 2.1; it has side length of 8λ, a grid of 40 points/λ and is surrounded by perfect matching layers of thickness 1λ on each side. More details on the simulations are given in Appendix 2.A.

2.3.1 2D scattering in the small hole approximation

We first consider the 2D scattering process, i.e. the scattering into waveguided modes. An example of cross section of the scattered field in the $z = 0$ plane is shown in Fig. 2.2. Figure Fig. 2.3 shows the calculated scattering efficiencies Q_{2D} for three single-mode slabs of different thickness; these are compared to the scattering efficiency calculated with Mie theory for an infinitely long hollow cylinder (n_1=1) in a volume filled with the same dielectric of the slab waveguide. We report data for both TM_0 and TE_0 modes.

As shown in Fig. 2.3, scattering efficiency for the hole increases with the thickness of the slab, approaching the value for the Mie case for the thicker slab. This behaviour can be understood by looking at the spatial distribution

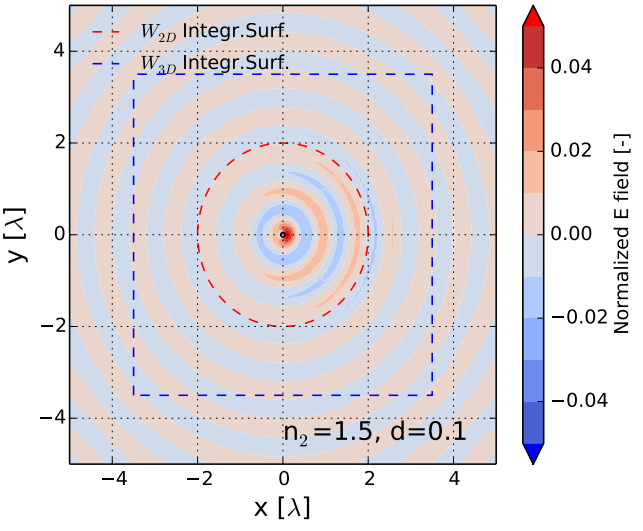

Figure 2.2: The calculated E_z component of the scattered electric field in the $z = 0$ plane for a hole diameter $d = 0.1\lambda$ and a waveguide thickness $h = 0.4\lambda$. The field is normalized to the amplitude of the incident E_z field. The red and blue dashed lines indicate the profiles of the surfaces for Poynting vector integration.

of the field that excites the hole: the fraction of the field that propagates inside the membrane increases with thickness, resulting in a stronger interaction with the dielectric discontinuity in the slab. We can quantify the fraction of the optical power inside the membrane using the confinement factor Γ ($0 < \Gamma < 1$) defined as:

$$\Gamma = \frac{\int_{slab} \vec{S'} \cdot \hat{x}\ dz}{\int \vec{S'} \cdot \hat{x}\ dz} \tag{2.3}$$

where $\vec{S'}$ is the time averaged Poynting vector and $\hat{x}$ the direction of propagation. Values of the confinement factors in our geometries are reported in Table 2.1, where we also report the polarization dependent ratios $R_Q^\mu = Q_{2D}/Q_{sca}$ for calculated scattering efficiency compared to the Mie case. As visible in Fig. 2.4, R_Q^μ shows a strong monotonic dependence on the confinement factor with a steep approach to the value of 1 for $\Gamma \to 1$; even for $\Gamma = 0.83$, $R_Q^\mu = 0.43$ in the TM case. This strong quantitative dependence is often not included when modelling disorder in membrane structures.

To check the dimensionality of our scattering problem, we fitted the calculated scattered efficiencies Q_{2D} with the polynomial dependence:

$$Q_{2D} = A\ r^p \tag{2.4}$$

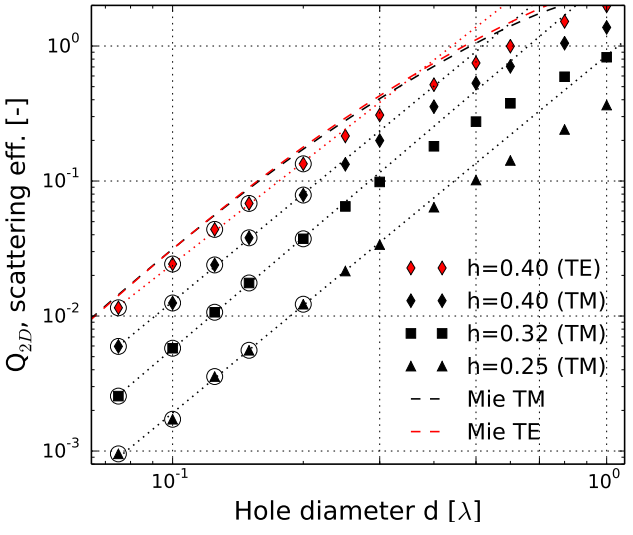

Figure 2.3: Calculated scattering efficiencies Q_{2D} as function of the diameter of the hole, for a slab refractive index of $n_2 = 1.5$. Data for TM_0 (in black) are plotted for three different thicknesses h in the single-mode regime. The TE_0 case (in red) is plotted only for the largest thickness. Polynomial fits $Q_{2D} = Ar^p$ were performed on data for $d \leq 0.2\lambda$ (encircled in the plot) and plotted as dotted lines. The scattering efficiencies of a Mie cylinder for TM and TE polarization, respectively shown in black and red dashed curves, have almost the same values in the examined diameters range.

with A and p as fitting parameters. The fit values reported in Table 2.1 are in the range $2.51 < p < 2.74$. The scattered power scales, in the 2D case, as $W_{2D} \propto r^4$ (induced dipole $\propto r^2 h$) and gives $Q_{2D} \propto r^3$ from Eq. (2.2). This is the 2D equivalent of the 3D scaling expected in the Rayleigh regime for small particles where $Q_{sph} \propto r^4$ ($W_{sphere} \propto r^6$). The results of the fit, giving p close to 3, indicate that a single hole scatters like a two dimensional system. We attribute the deviations of p from the expected value to the fact that the diameters used in the fit ($d < 0.2$) are not strictly in the limit of small-hole.

2.3.2 2D and 3D scattering

Next we report on the calculations of the power W_{3D} emitted outside the slab by the scattering hole. For this we integrate the z component of the time-averaged Poynting vector $\vec{S}'$ on a surface in proximity of the slab and parallel to the interface (see Appendix 2.A for more details). From W_{3D} we obtain the scattering efficiency Q_{3D} using Eq. (2.2).

Figure 2.5 reports the relative strength Q_{3D}/Q_{2D} of the 3D scattering

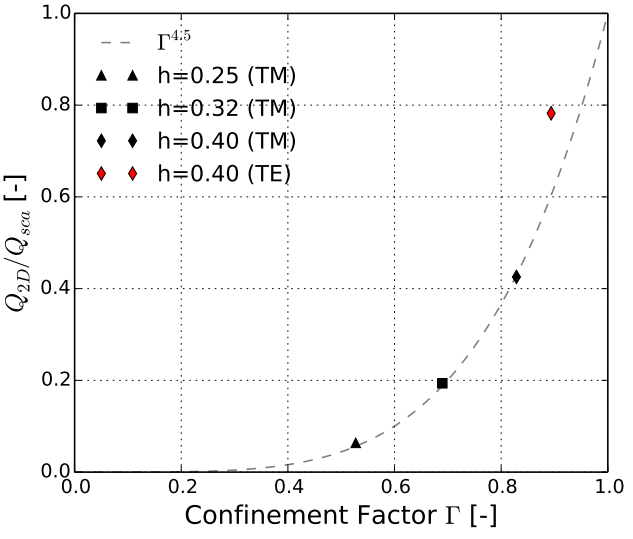

Figure 2.4: The ratio of Q_{2D} and the scattering efficiency of Mie cylinder Q_{sca} for different confinement factors (see text). The dashed line $\Gamma^{4.5}$ is an empirical fit added to guide the eye.

Table 2.1: Fit parameters of Q_{2D} shown in Fig. 2.3. p is the exponent of the polynomial dependence of the 2D scattering efficiency from the diameter of the hole (see Eq. (2.4)). Γ is the confinement factor for the slab mode defined in Eq. (2.3).

	h=0.25 (TM)	h=0.32 (TM)	h=0.40 (TM)	h=0.40 (TE)
p	2.65±0.17	2.74±0.05	2.65±0.06	2.51±0.07
Γ	0.53	0.69	0.83	0.89
R_Q^μ	0.06	0.19	0.43	0.78

process with respect to the 2D scattering process showing that the ratio of the two scattering efficiencies decreases with increasing thickness of the slab. This is expected as the guided light is more confined in a thicker membrane, and as a consequence less field is present at the facets of the cylinder and scattered in 3D. The values for the ratios Q_{3D}/Q_{2D} are relatively constant over the simulated hole diameters, with some variations in the range of hole sizes we investigate. These variations are not expected in the approximation where the hole scatters like a point dipole in the center of the slab [28] and are a first indication that our scattering system might be more complicated than expected.

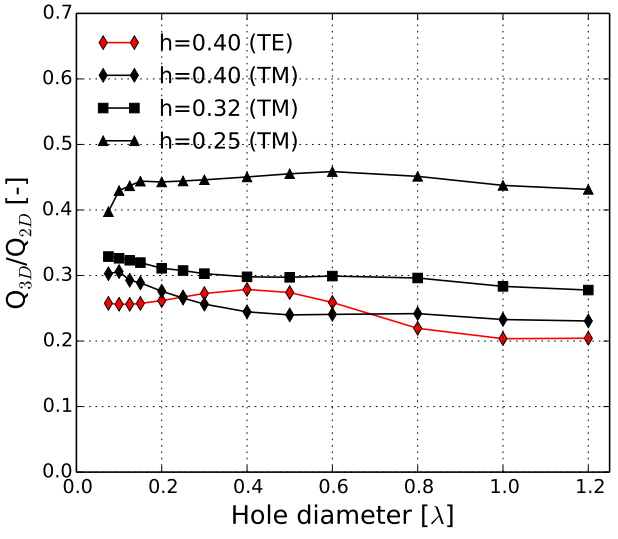

Figure 2.5: Ratio Q_{3D}/Q_{2D}, quantifying the scattering losses out of the slab relative to the scattering into slab modes, as function of the hole diameter d. Results are reported for the TM mode for $h = 0.40, 0.32, 0.25$ and for the TE mode for a slab thickness of $h = 0.40$.

We also simulate scattering from a single hole in slabs of higher refractive index for slab thickness h $= 0.25, 0.4$. The results show that for $n_2 = 3.4$ (typical of GaAs) the ratio of Q_{3D}/Q_{2D} decreases considerably to values $Q_{3D}/Q_{2D} \simeq 0.1$ for $h = 0.25$ and $Q_{3D}/Q_{2D} \simeq 0.03$ for $h = 0.4$, which is a factor 5 to 10 smaller than the ratio shown in Fig. 2.5. This is expected, as the largest refractive index will promote optical emission into the slab and reduce the relative emission to outside modes. We will not discuss these results any further, as they were obtained for thickness where the high-index slab supports multiple guided modes. The simulations for thinner slabs of high-index material proved to be too demanding for now.

2.3.3 Angular dependence of the 2D scattering

In the previous sections we have considered the total scattering cross section for the 2D and 3D scattering process. We now examine the angular properties of the 2D scattering, i.e. the differential scattering cross section $\sigma'(\theta) = d\sigma/d\Omega(\theta)$, with θ the scattering angle between the propagation direction of incident and scattered fields.

We calculate the intensity $I_s(\theta)$ scattered in the slab at a specific

angle and derive the normalized differential scattering cross section as $\hat{\sigma}'(\theta) = I_s(\theta)/\max(I_s(\theta))$. This allows to compare directly the angular dependence of the scattering function for holes of different diameters. We use the infinite Mie cylinder as reference, applying the same normalization to its scattering cross sections.

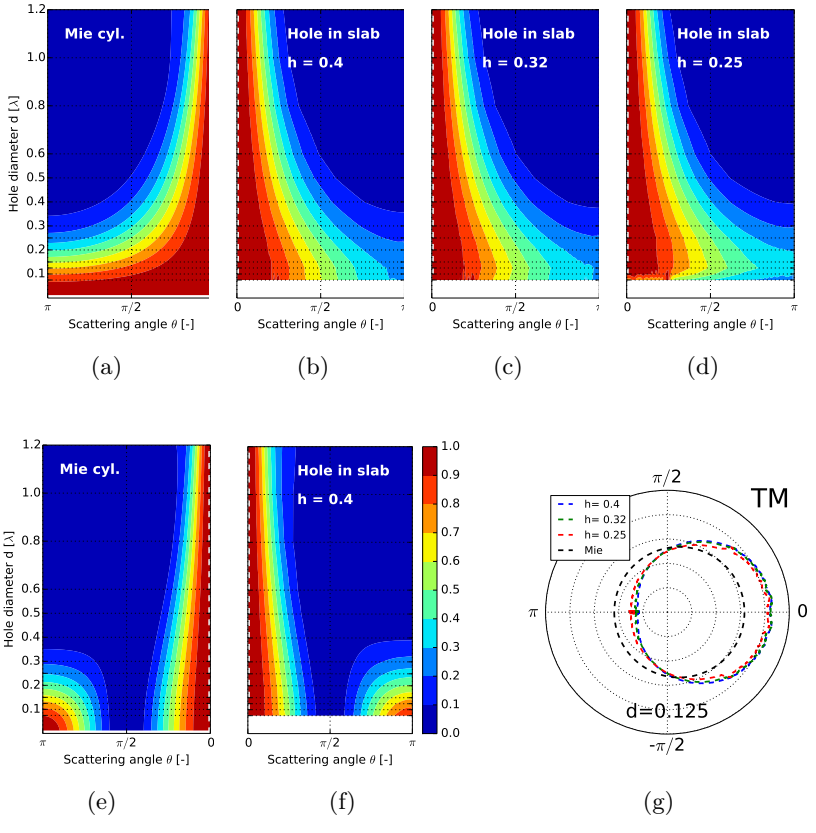

Figure 2.6: Normalized differential scattering cross sections $\sigma'(\theta)$ for TM (a-d) and TE (e-f) polarization, for Mie cylinders (a, e) and holes in slabs with $n_2 = 1.5$ and thickness h. The differential scattering cross section are all normalized to 1 and the colorscale defines ten bands for values from 0 to 1. The grid for the vertical axis indicates the values of hole diameters used in the simulations. $E_z(z = 0)$ for $h = 0.4$, $d = 0.1$ in TM case is shown in Fig. 2.2. In g) we report in polar coordinates the normalized differential scattering cross sections for holes of the same diameter $d = 0.125$ and slabs of three different thickness for TM polarization. The scattering in the slab geometries is more directional as compared to the corresponding Mie cylinder.

Figure 2.6 resumes the findings from the previously discussed simulations. We report on the left side the expected normalized $\sigma'(\theta)$ for a Mie cylinder and on the right the results for single holes in slabs of different thickness. In the TE case the scattered intensity shows two lobes centred around $\theta = 0, \pi$, as one would expect for a dipole oriented in the plane of the slab. We notice a striking difference in TM polarization between the angular scattering of a 2D Mie cylinder and a single hole. For Mie cylinders the normalized $\sigma'(\theta)$ tends to a constant value for $r \ll \lambda$, as expected for the dipole limit in the Rayleigh regime. Instead, for holes in confined geometry $\sigma'(\theta)$ shows a different behaviour, with more forward scattering in the limit of small holes. This surprising results indicates that the hole in a slab is more complex than a simple electric dipole with polarizability proportional to the hole volume. We speculate that the calculated reduced back scattering could originate from a more complicated polarization profile around the hole than one might expect from a first Born approximation of the scattering problem.

2.4 Relevance in modelling 2D random media

Our results have consequences in the calculation of transport properties of two-dimensional random scattering media. The cross sections we calculate for the single hole have direct equivalents for an infinite cylinder: σ_{2D} maps onto the scattering cross section σ_{sca} of the cylinder, whilst our σ_{3D} acts as an effective absorption cross section σ_{abs}, such that the total extinction cross section is $\sigma_{ext} = \sigma_{sca} + \sigma_{abs} = \sigma_{2D} + \sigma_{3D}$.

We suggest that it is possible to use 2D FDTD calculation to approximate the scattering of holes in a slab provided that two effects are accounted for. First, the scattering cross section calculated for Mie cylinder should be reduced by a factor R_Q^μ by rescaling the hole size to a diameter d_r, such that $\sigma_{sca}(d_r) = R_Q^\mu(h)\sigma_{sca}(d)$, where we indicate the dependence of R_Q^μ from the slab thickness which can be calculated with a single full 3D FDTD simulation. Secondly, an absorption cross section must be introduced to account for the out of plane losses. This can be achieved by adding an imaginary component to the refractive index of the material filling the hole $n_r = n_1 + in'$ such that $\sigma_{abs}(d_r, n_r) = \left(\frac{Q_{3D}}{Q_{2D}}\right)(h)\ \sigma_{sca}(d_r)$. The value of n' can be found numerically using analytical theory for Mie scattering. The proposed transformations are intended as approximations hinging on the assumption that a plane wavefront excites the hole. They offer the advantage that holes in a slab of thickness h

can be modelled with one full 3D FDTD simulation and calculations based on Mie scattering. These considerations also apply to the description of scattering in disordered 2D photonic crystal lattices [9].

To calculate the macroscopic transport properties of a 2D scattering medium we need to relate them to the microscopic scattering properties of the single hole. The scattering mean free path ℓ_{sca} can be calculated as $\ell_{sca}^{-1} = \rho\sigma_{sca}$ [9], with ρ the density of scatterers per unit surface. This expression is only valid for isotropic scattering; for anisotropic scattering $\sigma'(\theta)$ is weighted by a factor $(1 - \cos(\theta))$, with θ the usual scattering angle [18]. The inclusion of this correction for our smallest holes to account for the dominant forward scattering gives, for h=0.4, a mean free path 1.3 times longer than for the Mie case.

2.5 Conclusions

In conclusion, we numerically investigate the scattering of light from a hole in a dielectric slab of varying thickness (single-mode) with full 3D FDTD simulations. We find that the 2D scattering process dominates over the 3D radiative losses, and that the relative losses Q_{3D}/Q_{2D} are smaller when the mode is more confined in the waveguide, varying only slightly with hole size. We confirm that the scattering from a hole in a single-mode slab is a two dimensional process, like for an infinite Mie cylinder. Scattering from a hole in a slab differs from Mie scattering for a reduced scattering cross section, effective losses originating from 3D scattering and an unexpected directionality.

By studying the angular dependence of the 2D scattering we also find that, in TM polarization, the hole scatters light predominantly to the forward direction also in the limit of small holes, whereas the dipole approximation predicts a uniform radiation pattern in the slab plane. We thus conclude that a dipole model is insufficient to describe the scattering for small holes in a confined geometry.

Finally, we translate our observations in the consequences they have for the modelling of scattering in 2D random media. Apart from the necessity to include loss in these models, both the reduced scattering efficiency and altered angular dependence of the scattering lead to an effective increase of the scattering mean free path. We suggest a transformation for size and optical properties of the hole allowing, with only one full 3D FDTD simulation, to perform computationally lighter calculations on 2D random structures.

2.A FDTD simulations

The 3D cubic simulation cell used for this work is depicted in Fig. 2.2; it has a side length of 8λ and a grid density of 40 points/λ along each direction. The cell is surrounded by perfect matching layers of thickness 1λ on each side, for a final 3D cell of $(400)^3$ points. Simulations were performed with the FDTD software MEEP on CPU Intel Xeon E5 2603 1.8GHz $\times$ 4, 64 GB of RAM, for a calculation time of approximately one hour for each combination of slab thickness and hole size.

In our simulations the TM mode is excited in the slab with a line-dipole source oriented parallel to the y axis in the symmetry plane of the slab (see Fig. 2.2). This allows us to generate a flat wavefront propagating with in plane wavevector along x. The thickness of the slab is chosen such that only one mode is supported for each polarization. The simulations are run for a number of cycles sufficient for the scattered field to reach the edges of the simulation cell.

The scattered field $\vec{E}_S$ is calculated by complex field subtraction $\vec{E}_S = \vec{E}_T - \vec{E}_I$, where $\vec{E}_T$ is the total field in the presence of the scatterer and $\vec{E}_I$ the total field in absence of a hole. A similar relation applies to the scattered magnetic field $\vec{H}_S$. To calculate the scattering efficiencies we calculate the time averaged energy flux obtained from the real part of Poynting vector $\vec{S}' = \frac{1}{2}\mathrm{Re}\left(\vec{E}_S \times \vec{H}_S^*\right)$.

We obtain the total in-plane scattered intensity by integrating the radial component of $\vec{S}'$ over a cylindrical belt of radius $\tilde{R} = 2\lambda$ and total height of 2λ, which is large enough to contain the full guided mode. The power scattered in the radiative modes is in turn obtained by integrating the component of $\vec{S}'$ normal to the slab over a square centred in the origin, with side 7λ and in close proximity with the slab interface.

The convergence of the simulations was checked by comparison with Mie theory in the case of a long cylindrical air holes in glass, for different radii, and under the excitation of a plane wave created by a two dimensional dipolar source. This simulations showed almost perfect agreement with calculations based on theory. Mie scattering calculations were performed using scripts based on the code available from Bohren-Huffman [22].

2.B Results for higher index contrast (GaAs)

Optical waveguides generally used in real photonic application are obtained out of semiconductors like Si, Si_3N_4 or GaAs for wavelengths in the infrared. These materials have a higher refractive index than glass (with $n \simeq 1.5$), as for instance GaAs with $n_{GaAs} \simeq 3.4$. To explore the scattering properties for a single hole in a situation with a higher refractive index contrast, we also performed simulations for a slab of refractive index $n_2 = 3.4$ in air, comparable to a free standing GaAs membrane. The values for the thickness of the membrane have a lower limit imposed by the grid resolution; the values we used for h determine a waveguide able to support more than one mode. The results in this conditions are more complicated to interpret and hence we only present them in this appendix. In Fig. 2.7 we report the fractional losses Q_{3D}/Q_{2D}; and we note that the obtained values around 3% or lower are much smaller than for the same thicknesses in the case of $n_2 = 1.5$. This is a consequence of the higher index contrast and consequent increased confinement of the field.

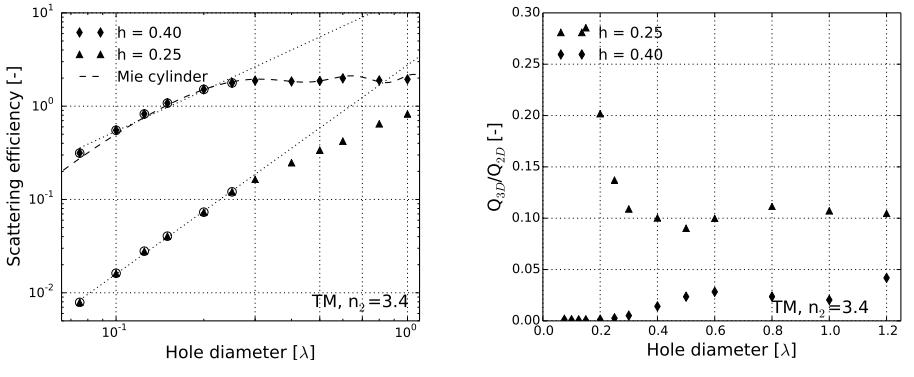

(a) (b)

Figure 2.7: Calculated scattering efficiencies Q_{2D} (left) and fractional loss Q_{3D}/Q_{2D} (right) for the TM_0 mode as function of the diameter of the hole, for a slab refractive index of n_2=3.4 and thickness h=0.25 and 0.4, both in the multi mode regime. Linear fit for datapoints with $d \leq 0.2\lambda$ (circled in the plot) is added in dotted line to highlight the polynomial dependence in the small particle regime. For comparison in dashed line the scattering efficiency of an infinitely long Mie cylinder.

In Fig. 2.8 we show the angular dependence of scattering from a hole in a high index slab. This appears to deviate from the simple dipolar prediction even more than for the case with $n_2 = 1.5$.

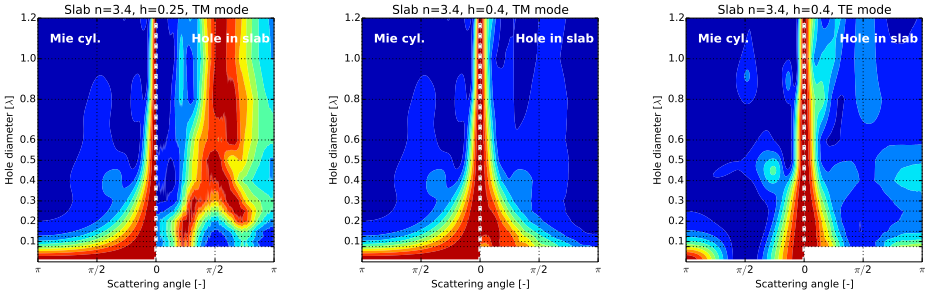

(a) TM, h=0.25 (b) TM, h=0.40 (c) TE, h=0.40

Figure 2.8: Angular dependence of the scattering from single hole in slabs with $n_2 = 3.4$ (GaAs) and different thicknesses. (a) h=0.25, TM case; (b) h=0.4, TM case; (c) h=0.4, TE case. Left side of the plots: normalized differential scattering cross sections of Mie cylinder. Right side of the plots: differential scattering cross sections calculated from FDTD simulations normalized to 1 for each hole diameter. The colorscale defines ten bands for values from 0 to 1. The grid for the vertical axis indicates the values of hole diameters used in the simulations.

Bibliography

[1] S. McNab, N. Moll, and Y. Vlasov, *Ultra-low loss photonic integrated circuit with membrane-type photonic crystal waveguides*, Opt. Express **11**, 2927 (2003).

[2] J. L. O'Brien, A. Furusawa, and J. Vučković, *Photonic quantum technologies*, Nat Photon **3**, 687 (2009).

[3] K. H. Madsen *et al.*, *Efficient out-coupling of high-purity single photons from a coherent quantum dot in a photonic-crystal cavity*, Phys. Rev. B **90**, 155303 (2014).

[4] J. D. Joannopoulos, P. R. Villeneuve, and S. Fan, *Photonic crystals: putting a new twist on light*, Nature **386**, 143 (1997).

[5] E. Yablonovitch, *Photonic band-gap structures*, J. Opt. Soc. Am. B **10**, 283 (1993).

[6] R. D. Meade, K. D. Brommer, A. M. Rappe, and J. D. Joannopoulos, *Existence of a photonic band gap in two dimensions*, Applied Physics Letters **61**, 495 (1992).

[7] S. G. Johnson, P. R. Villeneuve, S. Fan, and J. D. Joannopoulos, *Linear waveguides in photonic-crystal slabs*, Phys. Rev. B **62**, 8212 (2000).

[8] C. Bonato *et al.*, *Far-field emission profiles from L3 photonic crystal cavity modes*, Photonics and Nanostructures - Fundamentals and Applications **11**, 37 (2013).

[9] A. F. Koenderink, A. Lagendijk, and W. L. Vos, *Optical extinction due to intrinsic structural variations of photonic crystals*, Phys. Rev. B **72**, 153102 (2005).

[10] S. G. Johnson *et al.*, *Roughness losses and volume-current methods in photonic-crystal waveguides*, Appl. Phys. B **81**, 283 (2005).

[11] W. Bogaerts, P. Bienstman, and R. Baets, *Scattering at sidewall roughness in photonic crystal slabs*, Opt. Lett. **28**, 689 (2003).

[12] W. Bogaerts *et al.*, *Out-of-plane scattering in 1-D photonic crystal slabs*, Optical and Quantum Electronics **34**, 195 (2002).

[13] H. Zhang *et al.*, *Effective medium theory for two-dimensional random media composed of core-shell cylinders*, Optics Communications **306**, 9 (2013).

[14] A. Kirchner, K. Busch, and C. M. Soukoulis, *Transport properties of random arrays of dielectric cylinders*, Phys. Rev. B **57**, 277 (1998).

[15] L. Labonté, C. Vanneste, and P. Sebbah, *Localized mode hybridization by fine tuning of two-dimensional random media*, Opt. Lett. **37**, 1946 (2012).

[16] S. Boscolo and M. Midrio, *Three-Dimensional Multiple-Scattering Technique for the Analysis of Photonic-Crystal Slabs*, J. Lightwave Technol. **22**, 2778 (2004).

[17] H. Benisty *et al.*, *Radiation losses of waveguide-based two-dimensional photonic crystals: Positive role of the substrate*, Applied Physics Letters **76**, 532 (2000).

[18] G. M. Conley *et al.*, *Light Transport and Localization in Two-Dimensional Correlated Disorder*, Phys. Rev. Lett. **112**, 143901 (2014).

[19] S. F. Liew *et al.*, *Transmission channels for light in absorbing random media: From diffusive to ballistic-like transport*, Phys. Rev. B **89**, 224202 (2014).

[20] K. Vynck, M. Burresi, F. Riboli, and D. S. Wiersma, *Photon management in two-dimensional disordered media*, Nat Mater **11**, 1017 (2012).

[21] J. D. Jackson, *Classical Electrodynamics* (Wiley) (2007).

[22] C. F. Bohren and D. R. Huffman, *Absorption and scattering of light by small particles*, 10 ed. (Wiley) (1983).

[23] J. Venermo and A. Sihvola, *Dielectric polarizability of circular cylinder*, Journal of Electrostatics **63**, 101 (2005).

[24] R. Ruppin, *Electromagnetic scattering from finite dielectric cylinders*, J. Phys. D: Appl. Phys. **23**, 757 (1990).

[25] A. V. Shchegrov, I. V. Novikov, and A. A. Maradudin, *Scattering of Surface Plasmon Polaritons by a Circularly Symmetric Surface Defect*, Phys. Rev. Lett. **78**, 4269 (1997).

[26] A. Taflove, *Computational Electrodynamics: The Finite-difference Time-domain Method* (Artech House) (1995).

[27] A. F. Oskooi *et al.*, *Meep: A flexible free-software package for electromagnetic simulations by the FDTD method*, Computer Physics Communications **181**, 687 (2010).

[28] H. P. Urbach and G. Rikken, *Spontaneous emission from a dielectric slab*, Physical Review A **57**, 3913 (1998).